Check for updates

Zika Virus Methyltransferase: Structure and Functions for Drug Design Perspectives

Bruno Coutard,[a] Karine Barral,[b] Julie Lichière,[a] Barbara Selisko,[a] Baptiste Martin,[a]
Wahiba Aouadi,[a] Miguel Ortiz Lombardia,[c] Françoise Debart,[d]
Jean-Jacques Vasseur,[d] Jean Claude Guillemot,[a] Bruno Canard,[a] Etienne Decroly[a]

Aix Marseille Université, CNRS, AFMB UMR 7257, Marseille, France[a]; Aix Marseille Université, CNRS, INSERM,
Institut Paoli-Calmettes, CRCM, Marseille, France[b]; Structural and Genomic Information Laboratory, UMR 7256
(IMM FR 3479) CNRS Aix-Marseille Université, Luminy Campus, Marseille, France[c]; IBMM, UMR 5247 CNRS,
Université de Montpellier, ENSCM, Department of Nucleic Acids, Montpellier, France[d]

ABSTRACT The *Flavivirus* Zika virus (ZIKV) is the causal agent of neurological disorders like microcephaly in newborns or Guillain-Barre syndrome. Its NS5 protein embeds a methyltransferase (MTase) domain involved in the formation of the viral mRNA cap. We investigated the structural and functional properties of the ZIKV MTase. We show that the ZIKV MTase can methylate RNA cap structures at the N-7 position of the cap, and at the 2'-O position on the ribose of the first nucleotide, yielding a cap-1 structure. In addition, the ZIKV MTase methylates the ribose 2'-O position of internal adenosines of RNA substrates. The crystal structure of the ZIKV MTase determined at a 2.01-Å resolution reveals a crystallographic homodimer. One chain is bound to the methyl donor (*S*-adenosyl-L-methionine [SAM]) and shows a high structural similarity to the dengue virus (DENV) MTase. The second chain lacks SAM and displays conformational changes in the αX α-helix contributing to the SAM and RNA binding. These conformational modifications reveal a possible molecular mechanism of the enzymatic turnover involving a conserved Ser/Arg motif. In the second chain, the SAM binding site accommodates a sulfate close to a glycerol that could serve as a basis for structure-based drug design. In addition, compounds known to inhibit the DENV MTase show similar inhibition potency on the ZIKV MTase. Altogether these results contribute to a better understanding of the ZIKV MTase, a central player in viral replication and host innate immune response, and lay the basis for the development of potential antiviral drugs.

IMPORTANCE The Zika virus (ZIKV) is associated with microcephaly in newborns, and other neurological disorders such as Guillain-Barre syndrome. It is urgent to develop antiviral strategies inhibiting the viral replication. The ZIKV NS5 embeds a methyltransferase involved in the viral mRNA capping process, which is essential for viral replication and control of virus detection by innate immune mechanisms. We demonstrate that the ZIKV methyltransferase methylates the mRNA cap and adenosines located in RNA sequences. The structure of ZIKV methyltransferase shows high structural similarities to the dengue virus methyltransferase, but conformational specificities highlight the role of a conserved Ser/Arg motif, which participates in RNA and SAM recognition during the reaction turnover. In addition, the SAM binding site accommodates a sulfate and a glycerol, offering structural information to initiate structure-based drug design. Altogether, these results contribute to a better understanding of the *Flavivirus* methyltransferases, which are central players in the virus replication.

KEYWORDS methyltransferase, RNA processing, Zika virus, flavivirus, protein structure-function

First identified in 1947 in Uganda, Zika virus (ZIKV) reemerged in Brazil in early 2015, and the virus has continued to disseminate to South and North America in 2016. More than 2 million suspected cases have been reported (1), and ZIKV is now considered a major public health threat by the World Health Organization (WHO). Whereas the bite of an infected *Aedes aegypti* mosquito is the main cause of ZIKV transmission, direct human-to-human transmissions by sexual contacts have also been reported (2). ZIKV infection was initially considered a minor infection, often asymptomatic, causing mainly Zika fever with rash, arthralgia, and conjunctivitis. However, this outbreak revealed that ZIKV infecting pregnant women can be transmitted to the fetus, causing fetal loss, microcephaly, and other serious brain defects in newborns (3). In addition, Guillain-Barre syndrome, a rare autoimmune disease affecting the peripheral nervous system, and other severe neurological disorders have also been associated with ZIKV infection in adults (4). In the absence of a vaccine and antiviral drugs, the only way to reduce virus transmission is to limit the propagation of *Aedes* mosquito vectors. In view of the current expanding outbreak, it is urgent to develop a vaccine and antiviral strategies blocking essential enzymes involved in ZIKV replication.

ZIKV belongs to the *Flavivirus* genus, which contains other important human pathogens such as dengue virus (DENV), West Nile virus (WNV), or yellow fever virus (YFV). Flaviviruses are enveloped viruses containing a single-stranded positive-sense RNA genome of around 11,000 nucleotides, which is decorated by a cap structure. The cap structure consists of a guanosine residue linked through a 5′-5′ triphosphate bond to the 5′ end of mRNA (GpppN) (5). In flaviviruses, the cap structure is methylated at the nitrogen in position 7 of the guanosine (cap-0 structure, or ^{m}GpppN) and at the 2′-oxygen atom (2′-O) of the N_1 ribose (cap-1 structure, or ^{m}GpppN$_m$) (6, 7). The N-7 methylation of the cap structure is essential for RNA stability and stimulates their translation into viral protein by recognizing the translation initiation factor eIF4E (8). The 2′-O-methylation of the cap structure was demonstrated to protect viral RNA from being recognized by host cell sensors such as RIG-I and MDA5 that stimulate the production of interferons (9–11). In turn, interferon-stimulated genes, such as IFIT-1, can detect miscapped RNA and restrict their translation into proteins (12, 13). DENV mutant viruses lacking N-7-methyltransferase (MTase) activity show strong replication defects in infected cells, whereas those altering the 2′-O-MTase activity show only attenuated phenotypes (7, 14), as most cell lines used in the laboratory for virus replication are deprived of the RIG-I/MDA5 antiviral pathway. In contrast, it was demonstrated that a 2′-O-MTase knockout virus barely replicates in infected mice and elicits a strong humoral and cellular antiviral response (15, 16). Thus, viral RNA capping represents an attractive antiviral strategy (17, 18) since it should inhibit viral replication and/or accelerate virus clearance upon stimulation of the innate antiviral response.

In *Flavivirus*, the genome replication is driven by NS5, the RNA-dependent RNA polymerase (RdRp), which is associated with other viral nonstructural proteins in a membrane-bound replication-transcription complex. In addition to the RdRp domain, NS5 also harbors an N-terminal MTase domain, which methylates the cap structure of nascent RNA at both the N-7 and 2′-O positions (6, 7). Initially, biochemical studies performed with recombinant NS5 proteins or MTase domains (NS5-MTase) of DENV, WNV and other flaviviruses have confirmed the 2′-O-MTase activity using short synthetic RNA substrates in the presence of the methyl donor *S*-adenosyl-L-methionine (SAM, or AdoMet) (6, 19). The N-7-MTase activity was next demonstrated using longer RNA, with an optimal activity detected when a RNA containing the highly conserved stem loop A (SLA) hairpin structure was used (7, 20). The DENV MTase domain was later reported to methylate the 2′-O-ribose position of internal adenosines of the RNA (21). Nevertheless, the role of these methylations is still poorly understood. The structures of several *Flavivirus* NS5-MTases have been solved (6, 7), and the structure of ZIKV MTase has recently been determined by Coloma et al. (22). They adopt a canonical MTase Rossmann fold with a seven-stranded β-sheet surrounded by four α-helices. The MTase core structure closely resembles the catalytic domain of other viral and cellular SAM-dependent MTases with a conserved SAM binding site in close vicinity of the conserved
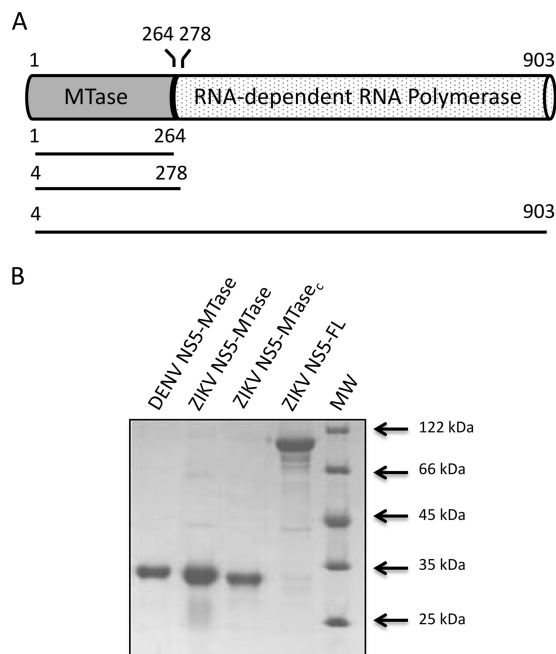
FIG 1 Purification of ZIKV NS5 2'-O-MTase. (A) The NS5 protein of ZIKV is a bifunctional protein with an MTase domain (N terminus) and an RdRp domain (C terminus). Two constructs, aa 4–903 and aa 4–278, were used for the functional studies, whereas construct aa 1–264 was used for crystallogenesis and structure determination. (B) The recombinant proteins were separated by SDS-PAGE and visualized by Coomassie blue staining prior their functional characterization. Arrows indicate the molecular mass markers.

K-D-K-E catalytic tetrad, the latter being a signature of 2'-O-MTases. In addition, structures determined in the presence of cap analogues, GTP or RNA reveal a cap binding pocket where the cap guanosine is held during 2'-O-methylation by stacking interactions with a phenylalanine (F24 residue in the DENV NS5 sequence) and an RNA binding zone where the RNA chain downstream of the cap structure is accommodated by a basic groove (4, 6, 7, 22–25).

Enzyme-based screenings or structure-based drug design have identified DENV, WNV, and YFV MTase inhibitors targeting either the SAM/SAH (S-adenosyl-L-homocysteine, the coproduct of the methylation) binding pocket (26–28), the cap binding pocket (29), or allosteric sites (30, 31). As ZIKV is closely related, we initiated a comparative study of ZIKV MTase with other *Flavivirus* MTases with the aim of subsequently developing original inhibitors or repurposing inhibitors targeting DENV MTase for antiviral research on ZIKV. Here we describe the structural and functional analysis of the ZIKV MTase domain as well as the evaluation of inhibitors developed for DENV MTase on ZIKV MTase.

RESULTS

Production and purification of ZIKV MTase constructs. The ZIKV genome encodes the bifunctional NS5 protein, with an ~264-amino-acid (aa) MTase domain at the N terminus followed by an RNA-dependent RNA polymerase (RdRp) domain (Fig. 1A). The MTase domain contains the canonical 2'-O-MTase (K-D-K-E) catalytic tetrad and possesses ~65% and 70% similarity to those of the four DENV serotypes and WNV, respectively. In this study, different constructs were designed. For functional assays, a construct, aa 4–278, encompassing the putative MTase domain from aa 4 to aa 278 of NS5, and full-length NS5 (aa 4 to 903) were produced and purified. From NS5 preparations, both the full-length protein and the MTase domain resulting from cleavage by bacterial proteases (here called NS5-MTase$_C$) were recovered after size exclusion chromatography (SEC). The purified proteins were detected as single bands at their expected molecular masses (~30 to 35 kDa and ~100 kDa, respectively) (Fig. 1B) upon

TABLE 1 Data collection and refinement statistics

Parameter	Value(s) for SAM complex[a]
Data collection and phasing statistics	
Space group	P1
Unit cell parameters	
a, b, c (Å)	37.6, 64.1, 72.0
α, β, γ (°)	113.1, 97.8, 92.0
Resolution range (Å)	65.41–2.01 (2.02–2.01)
No. of unique reflections	40,055 (398)
Completeness (%)	99.3 (93.9)
Multiplicity	3.3 (2.5)
R_{meas}[b]	0.157 (0.454)
$I/\sigma\langle I\rangle$	5.8 (2.0)
Refinement statistics	
Resolution range (Å)	65.41–2.01
No. of reflections:	
Used for refinement	40,054
Used for R_{free} calculation	2,105
R_{work} (%)[c]	16.0
R_{free} (%)[d]	19.1
No. of atoms	
Protein chain A	2,077
Protein chain B	1,963
Ligand/ion (SAM/glycerol/others)	27/6/21
Water	375
B factors (Å²)	
Protein chain A	28.0
Protein chain B	28.2
Ligand/ion (SAM/glycerol/others)	25.3/49.5/80.1
Water	37.9
RMSD from ideality	
Bond lengths (Å)	0.010
Bond angles (°)	0.96
Ramanchandran plot (%)	
Residues in most favored regions	97.40
Residues in disallowed regions	0

[a]Values in parentheses are for the outermost resolution shell of data.
[b]$R_{meas} = \Sigma|I_{obs} - I_{av}|/\Sigma I_{av}$, over all symmetry-related observations.
[c]$R_{work} = \Sigma|F_{obs} - \langle|F_{calc}|\rangle|/\Sigma|F_{obs}|$, over all reflections included in the refinement.
[d]R_{free} is calculated with 5% of reflections excluded from the refinement. In this formula, $\langle|F_{calc}|\rangle$ denotes the expectation value of $|F_{calc}|$ under the probability distribution used to define the likelihood function that is maximized in the refinement.

SDS-PAGE analysis. The apparent molecular mass observed for NS5-MTase$_C$ is similar to those of the ZIKV and DENV MTase domains (Fig. 1B).

ZIKV MTase crystallizes as a homodimer in which the two protomers show conformational differences. As the original MTase construct (aa 4–278) did not crystallize, we generated another that includes the complete N terminus but is devoid of the linker between the MTase and RdRp domains (aa 1–264; PDB code 5M5B). This construct allowed determination of the crystal structure of the ZIKV MTase domain. The structure was solved by molecular replacement using the DENV3 NS5 MTase/SAM (PDB code 3P97) as the template model and refined to a resolution of 2.01 Å, with R_{work} and R_{free} values of 16.0% and 19.1%, respectively. The crystal belongs to space group P1 with the following unit cell parameters: a = 37.6 Å, b = 64.1 Å, and c = 72.0 Å and α = 113.1°, β = 97.8°, and γ = 92.0°. Data collection and refinement statistics are reported in Table 1. The ZIKV MTase domain crystallized with two molecules in the asymmetric unit (Fig. 2A), whereas size exclusion chromatography indicates that the protein behaves as a monomer in solution. The low-interaction surface area (about 500 Å²) suggests that dimerization occurs during crystallization as previously observed for Modoc virus (MODV) MTase (32). The two protomers (A and B chains) are similarly folded, with significant differences arising from disorder in residues 43 to 58 of chain B (Fig. 2A). A superimposition of 244 Cα atoms in the A and B chains of the protein
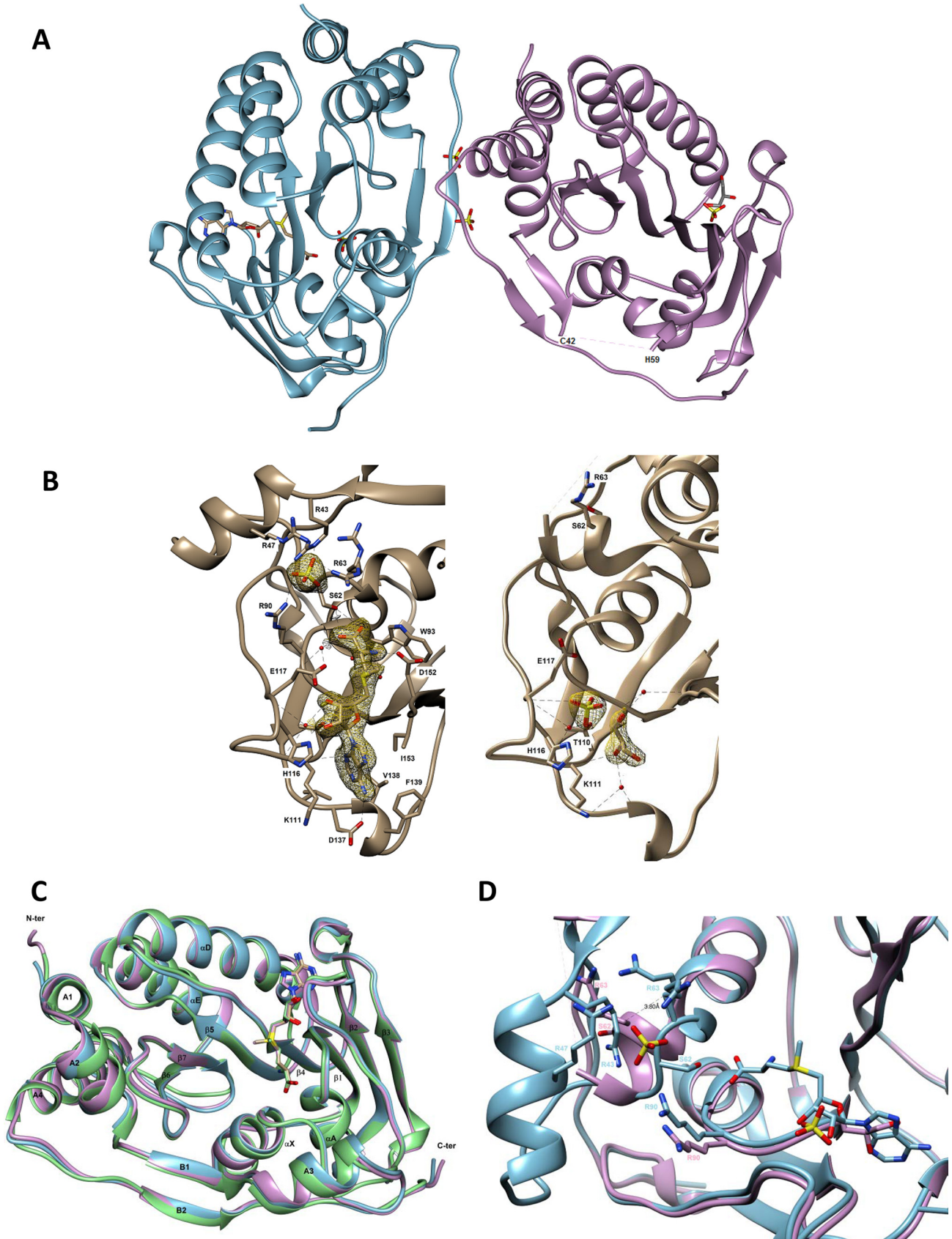
FIG 2 Crystal structure of ZIKV NS5-MTase. (A) Crystal structure of the ZIKV MTase two monomers (A and B chains). ZIKV MTase is drawn as a ribbon: chain A is colored blue, and chain B is colored pink. (B) To the left is shown the structure of the ZIKV MTase chain A in complex with the cofactor SAM and a

(Continued on next page)

resulted in an RMSD of 0.52 Å. Chain A consists of a canonical MTase core (residues 61 to 229, construct numbering PDB code 5M5B) folded into a seven-stranded β-sheet (β1 to β7) surrounded by four α-helices (αX, αA, αD, and αE), as shown in Fig. 2A and C. Appended to the core are an N-terminal extension (residues 8 to 60) and a C-terminal extension (residues 230 to 272). The N-terminal subdomain comprises a helix-turn-helix motif followed by a β-strand and an α-helix (A1, A2, B1, and A3). The C-terminal subdomain consists of an α-helix followed by a β-strand (A4 and B2). Inspection of the electron density maps reveals strong additional electron density in the SAM binding pocket, allowing the unambiguous modeling of SAM. Because no SAM is added during purification or crystallization, its presence in the structure must have originated from *E. coli*. The SAM molecule is bound in the central cleft formed of β-strands β1, β2, and β4 and α-helices αX and αA (Fig. 2A and B). The SAM adenine base is accommodated within a hydrophobic pocket defined by the side chains of Val138, Phe139, and Ile153 and stabilized by hydrogen bonds with a carboxylic oxygen from Asp137 and the nitrogen main-chain atoms of Lys111 and Val138 (Fig. 2B, left panel). The ribose moiety is hydrogen bonded to the Glu117 carboxyl group. The sugar is also bridged via a water molecule to the side chain of Glu117. The methionine tail of the SAM molecule is positioned by interactions with the side chains of Ser62, Trp93, and Asp152, as well as with the main chain of Gly92. The methionine carboxylate is also bridged via a single water molecule to the side chain of Glu117 and to the backbone of Arg90. Three molecules of sulfate interact with chain A. One of them is bound via a cluster formed by arginines Arg43, Arg47, Arg63, and Arg90 (Fig. 2D). The structure of chain A is highly similar to those of DENV-3 MTase (RMSD of 0.79 Å with PDB code 3P97 chain A) and of ZIKV MTase recently determined by Coloma et al. (RMSD of 0.29 Å with PDB code 5KQR chain A) (22). There is no difference in SAM binding with the latter structure (PDB code 5KQR), and the sulfate bound via a cluster formed by arginines Arg43, Arg47, Arg63, and Arg90 overlaps perfectly with the phosphate described by Coloma et al. (22). Structural differences from DENV-3 MTase are limited to small changes in the conformation of three solvent-exposed loops (residues 55 to 58, 178 to 183, and 251 to 254), as shown by superimposition of several structures (Fig. 2C).

We observe significant conformational changes between chain A and chain B of ZIKV MTase (RMSD of 0.52 Å) likely favored by their different crystal environments. Indeed, the chain B environment does not allow this loop to adopt the conformation observed in chain A. However, it is unlikely that crystal packing is the only factor involved since similar disorder has been observed, under different crystal packing, for the MODV MTase (PDB code 2WA2) (32). We conclude that the intrinsic flexibility of this loop, at least in the absence of the RNA substrate, has also contributed to building of this crystal form. As illustrated in Fig. 2A and D, three main differences are noteworthy in chain B, as follows. (i) There is no supporting electron density for residues 43 to 58 (part of the B1 β-strand, the A3 α-helix, and the following loop (Fig. 2A]). A similar absence of electron density has already been described for one of the two chains of the MODV MTase (32), suggesting a certain degree of flexibility in this region. (ii) Downstream of the aa 43–58 flexible region, the αX α-helix is kinked (Fig. 2D), with its N-terminal part (residues 61 to 67) taken away from this helix axis. (iii) There is no additional electron density characterizing the methyl donor SAM in the SAM binding site. Interestingly, in chain B of the MODV MTase, a SAM molecule is present, even if the

FIG 2 Legend (Continued)
sulfate ion. To the right is shown the structure of ZIKV MTase chain B in complex with glycerol- and sulfate-bound molecules. ZIKV MTase is drawn as a ribbon and colored gray. Small red spheres represent water molecules around the binding sites. Hydrogen bond interactions are shown as black dotted lines. The amino acid residues shown are those establishing Van der Waals interactions with bound molecules. In the insets, electron density maps are shown as a yellow mesh contoured at 1.5 σ around bound molecules. (C) Superposition of the ZIKV MTase chain A (PDB code 5M5B [in blue]), of the ZIKV MTase described by Coloma et al. (22) (PDB code 5KQR [in pink]), and of the DENV MTase (PDB code 3P97 [in green]) structures bound with SAM. (D) Superposition of ZIKV MTase chain A (drawn as a blue ribbon) and of ZIKV MTase chain B (drawn as a pink ribbon). Shown is a view of the cluster formed by arginines Arg43, Arg47, Arg63, and Arg90 and of the SAM binding site. The distance between Arg63 from chain A and chain B is shown as black dotted lines. For panels A through D, MTases are drawn as ribbons. The small molecules, SAM, glycerol, and sulfate ions are shown in cylinder representation with gray indicating the carbon atom. Nitrogen, oxygen, and sulfur are colored blue, red, and yellow, respectively.

homologous region aa 35–56 appears to also be disordered. However, the kink observed in the αX α-helix of ZIKV MTase chain B is absent from MODV MTase chain B. The kink has two main structural consequences. First, the side chain of Ser62 cannot interact anymore with the methionine tail of the SAM, as observed in chain A (Fig. 2B, left panel). Second, a cluster formed by arginines of the RNA binding groove (Arg43, Arg47, Arg63, and Arg90) in chain A is distorted in chain B and does not accommodate any sulfate molecule (Fig. 2D). In the absence of SAM, two polar molecules, a sulfate and a glycerol close by ($\sim$3.2 Å), are held in the SAM binding pocket of chain B (Fig. 2A and B). The sulfate molecule is positioned by hydrogen bonds with the side chain of His116, the main chain of Glu117, and with the bound glycerol nearby. It is also bridged via a single water molecule to the main chains of Gly112 and Glu117, as well as to the side-chain hydroxyl of Thr110. Moreover, the glycerol molecule participates in van der Waals interactions with the main chains of Gly87 and Lys111 and is stabilized by hydrogen bonds with the sulfate and the main-chain amide of Lys111. The glycerol is also bridged via two water molecules to the main chains of Asp137 and Val138 for the first one and to the main chains of Gly87 and Asp152 for the second one. Such a structure with compounds bound in the SAM binding site could serve as a basis for structure-based drug design.

Full-length ZIKV NS5 displays a 2′-O-MTase activity that is not regulated by the polymerase domain. The 2′-O-MTase activity was measured comparatively using the three ZIKV proteins (Fig. 1B). Proteins were incubated with a short RNA substrate bearing an unmethylated cap structure, GpppAC$_4$, in the presence of a radiolabeled methyl donor ([^{3}H]SAM). The amount of [^{3}H]CH$_3$ transferred onto RNA was quantified with a DEAE filter binding assay. ZIKV NS5, NS5-MTase$_C$, and the ZIKV NS5-MTase domain exhibit similar enzymatic activities (Fig. 3A). The level of detected enzymatic activities is about 30% lower than the control activity of DENV NS5-MTase. ZIKV NS5-MTase activity is thus not stimulated by the presence of the RdRp domain in *cis*. In addition, we compared the enzymatic activity of the ZIKV MTase domain using the unmethylated substrate GpppAC$_4$ and a substrate methylated at the N-7 position, ^{m}GpppAC$_4$. The methyl transfer efficiency is similar (Fig. 3B), suggesting that both substrates can be methylated at the 2′-O position of the adenosine ribose, as already reported for DENV and WNV MTases (19, 33). Additionally, the ZIKV MTase domain shows an optimal activity between pH 8 and 9 (Fig. 3C). Time course experiments indicate that the 2′-O-MTase functions without additional magnesium (not shown). We next addressed sequence specificity using short RNAs consisting of the 5′ ends of various viral RNAs starting either with A or G (Fig. 3D). Although RNA methylation efficiency by ZIKV MTase varies, we could not observe any obvious preference for *Flavivirus* GpppA-RNAs or GpppG-RNAs.

The ZIKV MTase requires long structured RNA to methylate the N-7 position of the cap. An SLA hairpin structure is present at the 5′ end of *Flavivirus* genomes. This structure is required for the detection of the N-7-MTase activity of WNV and DENV (7, 20). First, we compared the 5′ ends of ZIKV and DENV. The seven first residues of the ZIKV RNA are strictly identical to those of DENV, and ZIKV RNA forms a hairpin structure similar to that of DENV. N-7-methylation assays driven by ZIKV NS5-MTase were thus conducted on SLA-containing DENV RNAs with various 5′-capped ends (GpppA-RNA$_{75}$, ^{m}GpppA-RNA$_{75}$, GpppA$_m$-RNA$_{75}$, and ^{m}GpppA$_m$-RNA$_{75}$). ^{m}GpppA-DENV$_{75}$ and GpppA$_m$-DENV$_{75}$ are both significantly better methylated than ^{m}GpppA$_m$-DENV$_{75}$ ($P < 0.001$), indicating that N-7- and 2′-O-methylations occur (Fig. 3E). In addition, the high methylation level observed with ^{m}GpppA-DENV$_{75}$ suggests that the 2′-O-methylation is more efficient than the N-7-methylation under the applied experimental conditions. Interestingly, MTase activity using RNA already methylated at the N-7- and 2′-O positions (^{m}GpppA$_m$-DENV$_{75}$) was also detected. This observation suggests that additional methylations downstream of the cap structure might occur (described below). Altogether, these results show that, as observed for other flaviviruses, the ZIKV MTase can perform cap 2′-O-methylation on short RNAs without sequence specificity, whereas
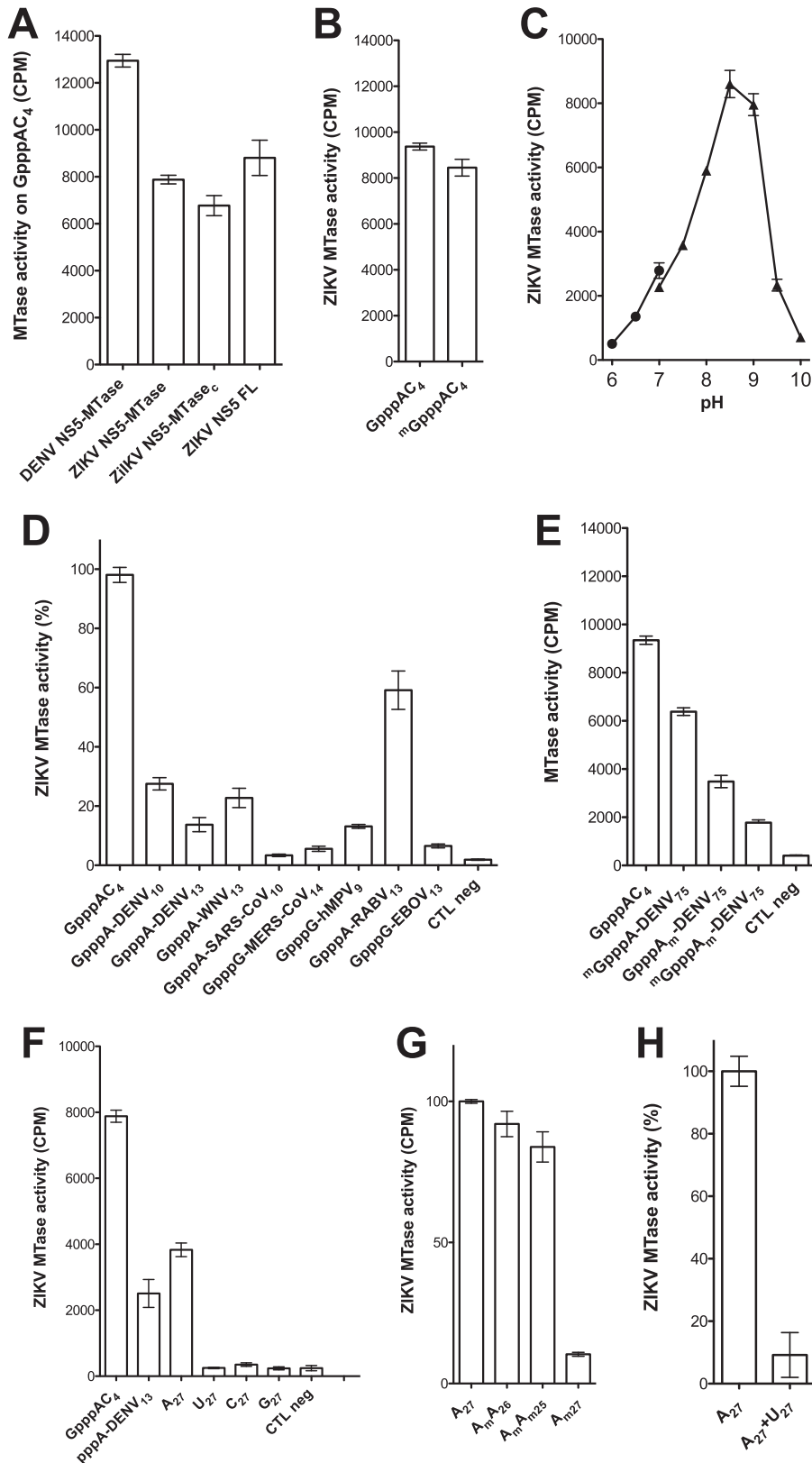
FIG 3 Characterization of the three MTase activities carried by ZIKV MTase. The ZIKV MTase activity was determined by monitoring the transfer of tritiated methyl groups (in counts per minute) from SAM to various synthetic RNAs. The bar graph presents the mean value and the standard deviation from 3 independent experiments. (A) Comparison of the MTase activities carried by the recombinant proteins using GpppAC$_4$ RNA as methyl acceptor. Shown is the enzymatic activity of ZIKV MTase domain on (B) small

(Continued on next page)

cap N-7-methylation does indeed require longer RNAs containing the *Flavivirus* conserved SLA structure.

The ZIKV MTase methylates single-strand RNA at the 2′-OH group of internal adenosines. Since the ZIKV MTase is active on double-methylated cap-1 RNAs (Fig. 3E), the methyl transfer on internal residues of RNAs was further investigated using uncapped RNAs in the presence of a 2-times-higher ZIKV MTase concentration than in the previous experiments. Figure 3F indicates that a 13-mer RNA bearing a 5′-triphosphate corresponding to the nascent 5′ end of DENV RNA can be methylated, confirming that ZIKV MTase methylates uncapped RNA putatively on internal positions. In order to further characterize this activity, homopolymeric RNAs bearing a 5′-OH group were tested (Fig. 3F). ZIKV NS5-MTase can methylate a 5′-OH-A_{27} RNA, but not 5′-OH-U_{27}, -G_{27}, and -C_{27} RNAs, indicating that ZIKV MTase methylates adenosine residues. Since ZIKV harbors a 2′-*O*-MTase catalytic tetrad, we inferred that the MTase activity targets the 2′-O of the ribose of the adenosine residues. This activity was confirmed by demonstrating that an RNA previously methylated at all 2′-O positions (A_{m27}), is not methylated by the ZIKV MTase (Fig. 3G). In addition, the internal adenosine 2′-O-methylation does not specifically occur in the vicinity of the RNA 5′ end since RNAs already methylated on the first (A_mA_{26}) or the two first ($A_mA_mA_{25}$) adenosines were methylated (Fig. 3G).
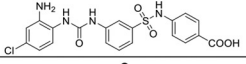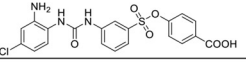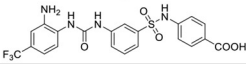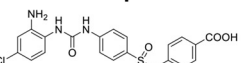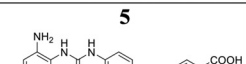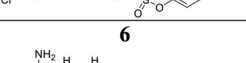
The 5′ ends of *Flavivirus* mRNAs are organized in an SLA structure, and many adenosines are engaged in double-strand stretches. We thus investigated whether the internal methylation could be selective for single-strand RNA (ssRNA) or double-strand RNA (dsRNA). We compared the MTase activities on A_{27} and on A_{27} previously annealed with a complementary U_{27} RNA. No MTase activity was detected using dsRNA (A_{27} + U_{27}) (Fig. 3H) confirming that ZIKV MTase methylates preferentially ssRNA. In conclusion, the ZIKV MTase preferentially methylates the 2′-O position of internal adenosine residues that are not involved in dsRNA structures.

Selected DENV MTase inhibitors show increased potency on ZIKV MTase. Our structural and biochemical analyses indicate that the ZIKV MTase shares common structural and functional characteristics with DENV MTase (RMSD of 0.79 Å for PDB code 3P97 chain A). We thus tested whether some compounds already documented to inhibit DENV MTase might also be active against the ZIKV MTase. SAM analogues and cap analogues were tested as well as allosteric inhibitors designed from a fragment-based screening campaign performed against DENV MTase (31). For this purpose, both internal methylation and cap 2′-O-methylation were monitored on GpppAC_4 and A_{27} RNA substrates, respectively, with increasing concentrations of the investigated inhibitors. We found that SAM analogues such as SAH and sinefungin inhibit cap-dependent ZIKV 2′-*O*-MTase activity with 50% inhibitory concentrations (IC$_{50}$) in the low micromolar range (Fig. 4A; Table 2). These compounds also abrogate internal methylation, but SAH shows a lower efficacy against internal methylation than sinefungin, which inhibits both methylations in a similar manner. Cap analogues (GpppA, ᵐGpppA, GpppG, and ᵐGpppG) bind to the DENV cap binding site by stacking interactions (34) and might therefore block RNA cap recognition, thus limiting cap methylation. This might also interfere with recognition and binding of uncapped RNA for internal methylation since the cap binding site might extend the RNA binding zone. GpppG and ᵐGpppG show more potent inhibitions than GpppA and ᵐGpppA on cap 2′-O-methylation, with IC$_{50}$ of 72 μM and 184 μM, respectively, versus 491 μM and 293 μM (Fig. 4B and C; Table 2). In addition, cap analogues inhibit internal methylations, to a lesser extent though, suggesting that the MTase cap binding site forms a part of the RNA binding zone but is not essential for internal methylation of an A_{27} RNA.

FIG 3 Legend (Continued)
GpppAC_4 and ᵐGpppAC_4 RNA, (C) 75 nucleotides of capped RNA with various 5′-end modifications (GpppA-RNA, ᵐGpppA-RNA GpppA$_m$A-RNA and ᵐGpppA$_m$A-RNA), (D) different uncapped RNAs, (E) uncapped poly(A) oligomers with various 2′-O-methylated positions (A_{27}, no methylation; A_mA_{26}, first position 2′-O-methylated; $A_mA_mA_{25}$, first and second positions 2′-O-methylated; A_{m27}, all positions 2′-O-methylated), and (F) ssRNA A_{27} and dsRNA A_{27}-U_{27}. CTL neg, enzymatic assay performed in the absence of RNA.

TABLE 2 Inhibition of the ZIKV 2'-O-MTase activity by various DENV MTase inhibitors[a]

	ZIKV 2'O-MTase activity IC$_{50}$ (µM)		DENV 2'O-MTase activity IC$_{50}$ (µM)
	GpppAC$_4$	A$_{27}$	GpppAC$_4$
SAH	0.43 ± 0.013	7.30 ± 0.44	0.34 ± 0.02
Sinefungin	1.18 ± 0.05	1.62 ± 0.08	0.63 ± 0.04
GpppA	491 ± 42	1082 ± 123	nd
mGpppA	293 ± 22	526 ± 47	nd
GpppG	72 ± 3.0	405 ± 22	nd
mGpppG	184 ± 8.0	351 ± 40	nd
1	221 ± 19	409 ± 47	452 ± 38
2	33.0 ± 2.7	138 ± 16	369 ± 14
3	24.0 ± 1.2	79.0 ± 16	91.0 ± 8.0
4	87.0 ± 9.7	168 ± 25	435 ± 26
5	31.0 ± 6.7	127 ± 22	368 ± 11
6	67.0 ± 5.1	230 ± 27	110 ± 11

[a]Shown is a summary of the IC$_{50}$ and the standard deviation (SD) deduced from Fig. 4 using the log (inhibitor) versus response variable slope equation and compared with the IC$_{50}$ previously published for DENV MTase. The IC$_{50}$ are an average from two to three independent measurements. nd, not determined.

Finally, we tested whether six compounds (1 to 6 in Table 2) targeting an allosteric site of DENV MTase (30, 31) could inhibit ZIKV MTase. All of the compounds selected on DENV MTase inhibit ZIKV cap 2'-O-MTase activity (Fig. 4D and Table 2). Compounds 1 to 6 exhibit lower IC$_{50}$ for ZIKV 2'-O-MTase activity than those for DENV MTase, suggesting that they are more potent on ZIKV MTase. In addition, all compounds inhibiting the cap-2'-O-MTase activity also inhibit the internal methylation, but with higher IC$_{50}$ (Table 2), indicating that internal and cap 2'-O-MTase activity use the same catalytic mechanism. These data also indicate that the structural and functional similarities between ZIKV and DENV MTase pave the way for the development of pan-viral inhibitors targeting the members of the *Flavivirus* genus.

DISCUSSION

The development of therapeutics against emerging arboviruses, such as ZIKV, is a major challenge. Acquisition of basic scientific knowledge on the emerging viral agent is often slow, whereas outbreaks can be sudden and unpredictable. In this work, we focus on the structure/function analysis of ZIKV NS5-MTase, closely related to that of DENV, and involved in the cap structure methylation. The latter is essential for viral RNA translation into proteins and the hiding of viral genomes from detection by cellular antiviral pathways (9, 15). The ZIKV MTase presented here crystallizes as a homodimer. Both protomers show a canonical MTase fold similar to those of DENV3 or WNV MTases, as well as those of other flaviviruses with SAM and cap binding sites close to the K-D-K-E catalytic tetrad. The first protomer of the ZIKV MTase crystallographic dimer
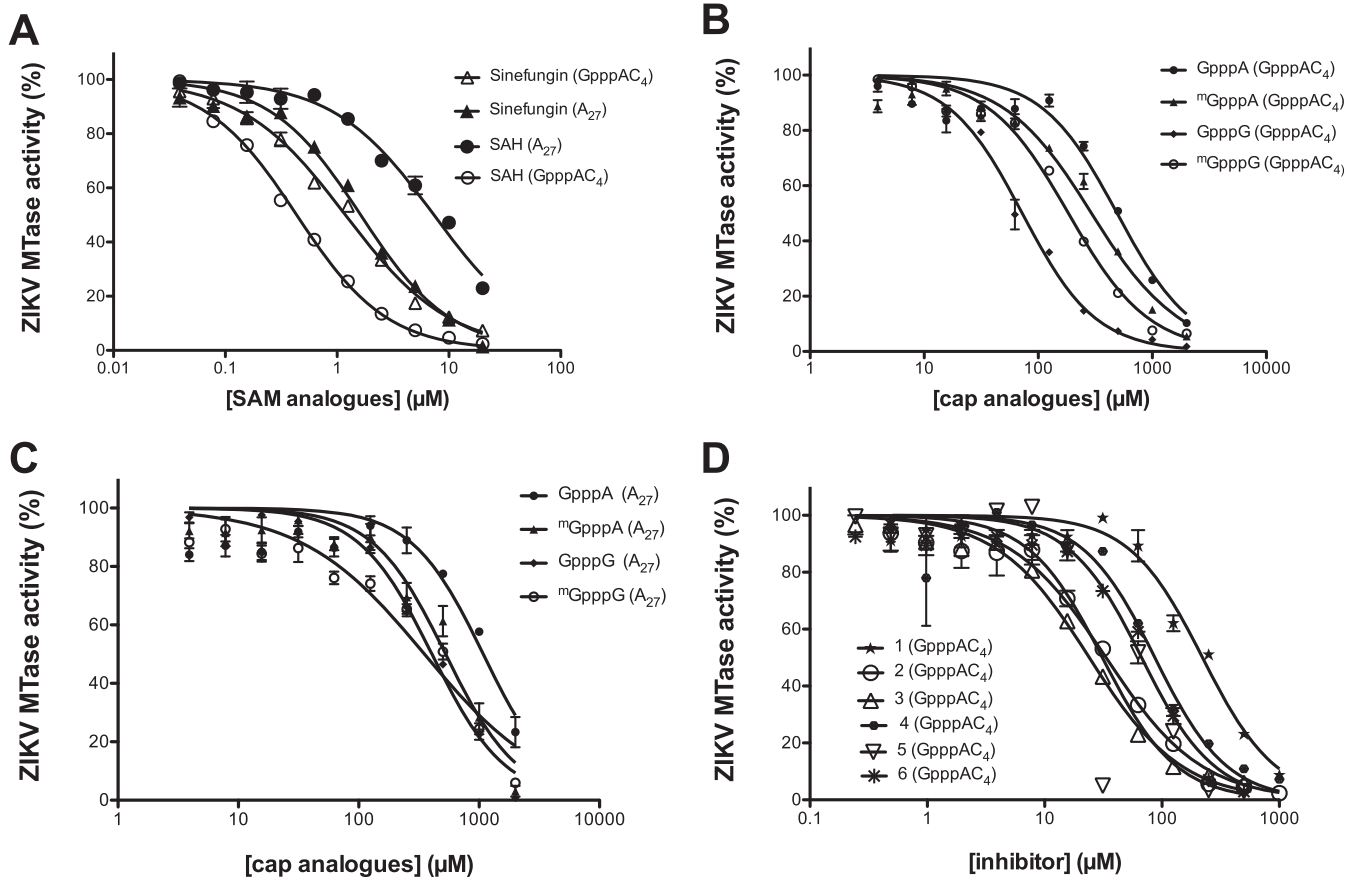
FIG 4 ZIKV MTase inhibition. The MTase assay was performed as indicated in Materials and Methods by incubating ZIKV NS5-MTase with GpppAC$_4$ (2'-O-cap methylation) or A$_{27}$ RNA (internal 2'-O-methylation). The methyl transfer onto RNA is measured by filter binding assay in the presence of increasing concentrations of inhibitors. The graph presents the mean value and standard deviation from 3 independent experiments. Shown is inhibition of cap 2'-O-MTase and internal methylation activity by (A) SAH and sinefungin, (B and C) cap analogues, and (D) compounds having allosteric inhibition (31).

contains the methyl donor SAM. It shows a high structural similarity to the ZIKV MTase structure recently determined by Coloma et al. (22). In this protomer, the SAM adenine base is held within a conserved hydrophobic pocket formed of β-strands β1, β2, and β4 and α-helices αX and αA. The leaving methyl group of the SAM is closely positioned to the catalytic site. The structure reveals that an arginine cluster, localized at the RNA binding site, binds a sulfate molecule (Fig. 2D). The homologous arginine residues were already reported to play a key role in the recruitment of RNA (25). Especially, residues corresponding to ZIKV MTase Arg63 and Arg90 (Arg57 and Arg84 in DENV, respectively) bind to the phosphate groups of the RNA during the 2'-O-methylation (25). The sulfate molecule bound via a cluster formed by arginines Arg43, Arg47, Arg63, and Arg90 (Fig. 2D) is closely located in between two phosphodiester groups of bound RNA in the structure described by Zhao et al. (25) (namely P3 U and P4 U from chain B, with distances for S-P3 of 3 Å and for S-P4 of 4 Å). In this cluster formed by arginines Arg43, Arg47, Arg63, and Arg90, the main chain of ZIKV MTase (chain A) and DENV MTase (chain B [23]) structures overlap perfectly. Only slight conformational changes are noted for some side chains (mostly Arg63 and Arg90) due to the accommodation of bound RNA. This slight difference in positioning between sulfate and phosphate is probably due to the fact that sulfate can accommodate more freely than RNA. We thus speculate that the sulfate identified in the ZIKV protomer A mimics a phosphate group of viral RNA and holds the arginines in an RNA-bound conformation. In chain B, these arginines are not organized in a cluster and the sulfate ion is absent, possibly mimicking the RNA-free enzyme (Fig. 2D). In this conformation, the region encompassing residues 43 to 58 is disordered and the αX helix is kinked, moving Arg63 away from the cluster. As

a consequence, Ser62 can no longer stabilize the SAM (or *S*-adenosyl-L-homocysteine [SAH]) molecule bound to the MTase. The structural differences between two protomers could thus provide possible snapshots of the ZIKV MTase after the recruitment of a capped RNA together with a SAM molecule (chain A) or after the release of the methylated capped RNA and the SAH molecule (chain B). This hypothesis would propose a key role for Arg63 in the enzymatic reaction turnover.

In addition, the structure highlights a hydrophobic cavity adjacent to the SAM binding site, which is conserved among *Flavivirus* MTases. This site can serve for structure-based drug design approaches. Indeed, this cavity can accommodate SAH derivatives substituted at the N6 position of the adenosine base, leading to inhibition of DENV MTase (27). The second protomer (chain B) presents significant differences. Instead a glycerol molecule and a sulfate ion were closely accommodated into the SAM binding site, providing a unique opportunity to serve as a basis for structure-based drug design and more especially for a "fragment-linking" strategy (35).

The functional characterization demonstrates that the ZIKV MTase harbors N-7 and 2'-*O*-methytransferase activities contributing to the formation of a cap-1 structure on the viral mRNA. The interface between the MTase and the RdRp domains has been reported to be essential for the replication regulation of dengue virus (36–38) or Japanese encephalitis virus (39). It is also known that the MTase domain contributes to an efficient initiation and elongation of the RNA polymerization by the dengue virus RdRp (40). Conversely, in this study, we show that the 2'-*O*-MTase activity of ZIKV MTase on short capped RNAs is not activated by the RdRp domains. However, it is noteworthy that our biochemical assay might not be optimal to look for a possible interplay between the two domains as the RNA used by the MTase is not neo-synthesized by the RdRp. As observed for its close relatives DENV and WNV, the 2'-*O*-MTase activity can be detected using different short RNA substrates with no obvious sequence specificity (19, 33). In contrast the N-7-MTase activity requires an RNA substrate forming a hairpin structure mimicking the SLA structure conserved among flaviviruses (7, 20). We infer that both cap N-7- and 2'-*O*-MTase activities play an essential role in the virus life cycle. The N-7-methylation of the viral RNA cap by ZIKV NS5-MTase allows recognition by the translation initiation factor eIF4E and stimulation of translation into viral proteins (8). On the other hand, 2'-*O*-methylation of the cap is expected to mask the presence of exogenous viral RNAs from host cell sensors such as RIG-I and MDA5 (9–11), which induce the production of interferons. In addition, 2'-O-methylation of viral RNA is thought to prevent translation restriction by interferon-stimulated genes (ISGs) such as the IFIT-1 gene (12, 13). Thus, molecules inhibiting ZIKV MTase activities are expected to translate into a strong antiviral effect (41). Apart from the RNA-cap MTase activities, we observed that ZIKV NS5-MTase also methylates the 2'-O position of adenosine residues located at internal positions of the RNA substrate. This activity is mainly detected on adenosine residues using homopolymeric ssRNAs but not dsRNAs, which barely interact with the ZIKV NS5-MTase. Similar internal methylation on adenosine residues was already reported for DENV MTase (21), but the role of such methylations is still elusive.

The close structural and functional similarity of ZIKV MTase to other *Flavivirus* MTases suggests that work previously made on DENV MTase may help in the development of antiviral compounds targeting ZIKV MTase. To further assess this, we evaluated three classes of DENV MTase inhibitors, cap analogues, SAM analogues, and allosteric inhibitors on ZIKV MTase. Our results show that these molecules can serve as a starting point to identify MTase inhibitors. As expected, we observe that cap and SAM analogues, already described to inhibit viral MTases, show a similar inhibitory effect on ZIKV MTase. However, when targeting the SAM binding site, the main challenge remains compound selectivity to avoid inhibition of cellular MTases. In this respect, the structure of ZIKV MTase reveals that a specificity increase might be achievable using the conserved hydrophobic cavity adjacent to the SAM binding site, as in the case of DENV MTase (27). Another option to develop selective compounds is to target allosteric—i.e., noncatalytic—sites. We thus tested compounds previously discovered using DENV MTase and targeting an allosteric site structurally conserved between ZIKV and DENV

enzymes (31). Similarly, higher inhibition effects were observed on ZIKV MTase cap 2′-O-MTase activity.

In summary, we present here the first structure/function study of the ZIKV MTase. This study reveals the high similarities between DENV and ZIKV MTase structures. In addition we also describe an original structure of the ZIKV MTase in the absence of SAM showing conformational changes in the RNA binding groove together with the SAM binding pocket. The comparison of both structures might reveal the molecular basis driving the enzymatic turnover of flavivirus MTases. Finally, we provide a strong basis for the development of small molecules targeting MTase activities carried by ZIKV NS5. This study highlights the need to improve the basic science knowledge and antiviral research on virus families with high emerging potential.

MATERIALS AND METHODS

Plasmid constructs. For the functional study, the coding sequence of ZIKV NS5 (aa 4–903) and the ZIKV NS5 MTase (aa 4–278) domain were synthesized (Genscript) based on the sequence of the ZIKV strain H/PF/2013 (GenBank accession no. KJ776791.2) and then cloned into a pQE30 (Qiagen) plasmid with an N-terminal His$_6$ tag. For the structural study, the coding sequence of ZIKV NS5 MTase (aa 1–264) was amplified by PCR starting from the synthetic gene and subcloned in pDEST14 (Thermo Fisher Scientific) with an N-terminal His$_6$ tag.

Expression and purification of NS5 and NS5-MTase domain proteins. The MTase domains (aa 4–278 and aa 1–264) were produced in *Escherichia coli* T7 Express Iq (New England BioLabs). Cells were grown in Terrific Broth at 37°C until the optical density at 600 nm (OD$_{600}$) reached 0.6. Protein expression was then induced by 0.5 mM IPTG (isopropyl-β-D-thiogalactopyranoside) at 17°C overnight. Bacteria were harvested by centrifugation. The bacterial pellets from a 2-liter bacterial culture were resuspended in 100 ml lysis buffer (50 mM Tris-HCl [pH 8], 300 mM NaCl, 5% glycerol, 0.1% Triton, 10 μg/ml DNase I, 2 tablets of EDTA-free antiprotease cocktail [Roche], 0.25 mg/ml lysozyme). After 30 min of incubation at 4°C, the cells were sonicated and clarified by centrifugation prior to immobilized metal affinity chromatography (IMAC) purification on a 5-ml His prep column (GE Healthcare), with elution in 50 mM Tris-HCl, 300 mM NaCl, and 250 mM imidazole (pH 8.0). The eluted protein was then loaded on a 16/60 Superdex 200 (GE Healthcare) equilibrated in a mixture of 10 mM HEPES, 500 mM NaCl, glycerol 5%, and 1 mM dithiothreitol (DTT [pH 7.5]).

The protocol for the production and purification of the ZIKV NS5 was adapted from the protocol developed for DENV NS5 (40). After the IMAC purification, a size exclusion chromatography (SEC) step was applied to separate the cleaved MTase and the full-length NS5 using a Superdex S75 HR 16/20 column (GE Healthcare) preequilibrated in a mixture of 50 mM HEPES (pH 7.5), 750 mM NaCl, 10% glycerol, and 10 mM DTT. Proteins were concentrated and stored at −20°C after adding glycerol to a final concentration of 40%.

Radioactive methyltransferase assay. The enzymatic assays were carried out in 40 mM Tris-HCl (pH 8.0), 1 mM DTT, 2 μM SAM, and 0.33 μM [^{3}H]SAM (PerkinElmer) in the presence of 0.7 μM synthetic RNAs with various 5′-end modifications (triphosphorylated, pppRNA; unmethylated cap, GpppARN; cap-0, ^{m}GpppARN, or 2′-O-methylated cap, GpppG$_m$RNA). Purified ZIKV NS5 and NS5-MTase were added to final concentrations of 0.75 μM, except for the internal methylation assay, which was performed in the presence of 1.5 μM MTase.

Reaction mixtures were incubated at 30°C and stopped after 30 min except for the time course experiments by a 10-fold dilution of the reaction mixture in 20 μM ice-cold SAH. Samples were then transferred to DEAE cellulose filters (PerkinElmer) by using a Filtermat Harvester apparatus (Packard Instruments). The unincorporated [^{3}H]SAM was removed from the filter by several washing steps with 10 mM ammonium formate (pH 8.0), with H$_2$O, and with absolute ethanol, before drying the DEAE filters. The filters transferred into plastic bags, BetaplateScint (Wallac) scintillation fluid was added before quantification of [^{3}H]methyl groups transferred onto RNA substrates in counts per minute using a Wallac 1450 MicroBetaTriLux liquid scintillation counter.

For the MTase inhibition assays, 0.75 μM ZIKV NS5-MTase was mixed with the inhibitor candidate before the addition of SAM and RNA substrate to start the reaction. The final concentration of dimethyl sulfoxide (DMSO) in the reaction mixtures was below 5%, and control reactions were performed in the presence of similar DMSO concentrations. Reaction mixtures were incubated at 30°C for 30 min and analyzed by filter binding assay as described above.

The IC$_{50}$s of SAH, sinefungin, cap analogues, and compounds 1 to 6 were determined with GraphPad Prism using the log (inhibitor) versus response variable slope equation.

Synthesis of RNA substrates. Various short RNA sequences were chemically synthesized on a solid support using an ABI 394 synthesizer. After RNA elongation with 2′-O-pivaloyloxymethyl phosphoramidite monomers (42) (Chemgenes, USA), the 5′-hydroxyl group of RNA still anchored to the solid support was phosphorylated, and the resulting *H*-phosphonate derivative was oxidized and activated into a phosphoroimidazolidate derivative to react with either pyrophosphate to give a 5′-triphosphate RNA (pppRNA) (43) or GDP to give GpppRNA (44). After deprotection and release from the solid support, the GpppRNA sequences were purified by ion-exchange–high-performance liquid chromatography (IEX-HPLC) and validated to be >95% pure by IEX-HPLC analysis, and they were unambiguously characterized by matrix-assisted laser desorption ionization–time of flight (MALDI-TOF) mass spectrometry. Subsequent N-7-methylation of the purified GpppRNAs was performed enzymatically using N-7-hMTase (44).

Crystallization conditions. The ZIKV MTase (aa 1–264) was concentrated to 5 mg/ml for crystallization screenings in sitting drops. After 2 weeks, crystals were obtained and optimized in 150 mM sodium citrate (pH 5.6) and 1.5 M ammonium sulfate. Crystals were transferred to a cryoprotectant solution of the same reservoir solution containing 10% glycerol for a few seconds and flash-cooled in liquid nitrogen.

Data collection, automated data processing, and refinement. Diffraction data were collected at the SOLEIL synchrotron (Proxima 1). We used AutoPROC (45) for data processing. Images were processed and scaled using XDS (46) and Aimless (47). Phaser (48) was used for molecular replacement. The structure of DENV3 NS5-MTase/AdoMet (PDB code 3P97) was used as the template model. The first ZIKV MTase model was built using ARP/wARP (49), and autoBUSTER (50) was used for structure refinement. Iterative cycles of model building were done with the program COOT (51). The quality of the refined structures was assessed with MOLPROBITY (52). The crystal structure was determined at a resolution of 2.01 Å and belonged to space group P1 with the following unit cell parameters: a = 37.6 Å, b = 64.1 Å, and c = 72.0 Å and α = 113.1°, β = 97.8°, and γ = 92.0°. Gesamt (53) was used to superimpose the obtained model with DENV3 MTase (PDB code 3P97), ZIKV MTase (PDB code 5KQR), and MODV MTase (PDB code no. 2WA1) and to determine RMSD values. Figures were generated with Chimera.

Accession number(s). The crystal structure of the Zika virus MTase construct generated in this study was deposited in the Protein Data Bank (PDB) under code 5M5B.

ACKNOWLEDGMENTS

REFERENCES

1. Walker WL, Lindsey NP, Lehman JA, Krow-Lucal ER, Rabe IB, Hills SL, Martin SW, Fischer M, Staples JE. 2016. Zika virus disease cases—50 States and the District of Columbia, January 1–July 31, 2016. MMWR Morb Mortal Wkly Rep 65:983–986. https://doi.org/10.15585/mmwr.mm6536e5.

2. Musso D, Roche C, Robin E, Nhan T, Teissier A, Cao-Lormeau VM. 2015. Potential sexual transmission of Zika virus. Emerg Infect Dis 21:359–361. https://doi.org/10.3201/eid2102.141363.

3. Ventura CV, Maia M, Bravo-Filho V, Góis AL, Belfort R. 2016. Zika virus in Brazil and macular atrophy in a child with microcephaly. Lancet 387:228. https://doi.org/10.1016/S0140-6736(16)00006-4.

4. Cao-Lormeau V-M, Blake A, Mons S, Lastere S, Roche C, Vanhomwegen J, Dub T, Baudouin L, Teissier A, Larre P, Vial A-L, Decam C, Choumet V, Halstead SK, Willison HJ, Musset L, Manuguerra J-C, Despres P, Fournier E, Mallet H-P, Musso D, Fontanet A, Neil J, Ghawche F. 2016. Guillain-Barre syndrome outbreak associated with Zika virus infection in French Polynesia: a case-control study. Lancet 387:1531–1539. https://doi.org/10.1016/S0140-6736(16)00562-6.

5. Decroly E, Ferron F, Lescar J, Canard B. 2011. Conventional and unconventional mechanisms for capping viral mRNA. Nat Rev Microbiol 10:51–65. https://doi.org/10.1038/nrmicro2675.

6. Egloff MP, Benarroch D, Selisko B, Romette JL, Canard B. 2002. An RNA cap (nucleoside-2′-O-)-methyltransferase in the flavivirus RNA polymerase NS5: crystal structure and functional characterization. EMBO J 21:2757–2768. https://doi.org/10.1093/emboj/21.11.2757.

7. Zhou Y, Ray D, Zhao Y, Dong H, Ren S, Li Z, Guo Y, Bernard KA, Shi P-Y, Li H. 2007. Structure and function of flavivirus NS5 methyltransferase. J Virol 81:3891–3903. https://doi.org/10.1128/JVI.02704-06.

8. Muthukrishnan S, Both GW, Furuichi Y, Shatkin AJ. 1975. 5′-Terminal 7-methylguanosine in eukaryotic mRNA is required for translation. Nature 255:33–37. https://doi.org/10.1038/255033a0.

9. Züst R, Cervantes-Barragan L, Habjan M, Maier R, Neuman BW, Ziebuhr J, Szretter KJ, Baker SC, Barchet W, Diamond MS, Siddell SG, Ludewig B, Thiel V. 2011. Ribose 2′-O-methylation provides a molecular signature for the distinction of self and non-self mRNA dependent on the RNA sensor Mda5. Nat Immunol 12:137–143. https://doi.org/10.1038/ni.1979.

10. Schuberth-Wagner C, Ludwig J, Bruder AK, Herzner AM, Zillinger T, Goldeck M, Schmidt T, Schmid-Burgk JL, Kerber R, Wolter S, Stümpel JP, Roth A, Bartok E, Drosten C, Coch C, Hornung V, Barchet W, Kümmerer BM, Hartmann G, Schlee M. 2015. A conserved histidine in the RNA sensor RIG-I controls immune tolerance to 2′O-methylated self RNA. Immunity 43:41–52. https://doi.org/10.1016/j.immuni.2015.06.015.

11. Devarkar SC, Wang C, Miller MT, Ramanathan A, Jiang F, Khan AG, Patel SS, Marcotrigiano J. 2016. Structural basis for m7G recognition and 2′-O-methyl discrimination in capped RNAs by the innate immune receptor RIG-I. Proc Natl Acad Sci U S A 113:596–601. https://doi.org/10.1073/pnas.1515152113.

12. Daffis S, Szretter KJ, Schriewer J, Li J, Youn S, Errett J, Lin T-Y, Schneller S, Zust R, Dong H, Thiel V, Sen GC, Fensterl V, Klimstra WB, Pierson TC, Buller RM, Gale M, Shi P-Y, Diamond MS. 2010. 2′-O methylation of the viral mRNA cap evades host restriction by IFIT family members. Nature 468:452–456. https://doi.org/10.1038/nature09489.

13. Kumar P, Sweeney TR, Skabkin MA, Skabkina OV, Hellen CUT, Pestova TV. 2014. Inhibition of translation by IFIT family members is determined by their ability to interact selectively with the 5′-terminal regions of cap0-, cap1- and 5′ppp-mRNAs. Nucleic Acids Res 42:3228–3245. https://doi.org/10.1093/nar/gkt1321.

14. Dong H, Chang DC, Xie X, Toh YX, Chung KY, Zou G, Lescar J, Lim SP, Shi PY. 2010. Biochemical and genetic characterization of dengue virus methyltransferase. Virology 405:568–578. https://doi.org/10.1016/j.virol.2010.06.039.

15. Li S-H, Dong H, Li X-F, Xie X, Zhao H, Deng Y-Q, Wang X-Y, Ye Q, Zhu S-Y, Wang H-J, Zhang B, Leng Q-B, Zuest R, Qin E-D, Qin C-F, Shi P-Y. 2013. Rational design of a flavivirus vaccine by abolishing viral RNA 2′-O methylation. J Virol 87:5812–5819. https://doi.org/10.1128/JVI.02806-12.

16. Züst R, Dong H, Li X-F, Chang DC, Zhang B, Balakrishnan T, Toh Y-X, Jiang T, Li S-H, Deng Y-Q, Ellis BR, Ellis EM, Poidinger M, Zolezzi F, Qin C-F, Shi P-Y, Fink K. 2013. Rational design of a live attenuated dengue vaccine: 2′-O-methyltransferase mutants are highly attenuated and immunogenic in mice and macaques. PLoS Pathog 9:e1003521. https://doi.org/10.1371/journal.ppat.1003521.

17. Ferron F, Decroly E, Selisko B, Canard B. 2012. The viral RNA capping machinery as a target for antiviral drugs. Antiviral Res 96:21–31. https://doi.org/10.1016/j.antiviral.2012.07.007.

18. Lim SP, Noble CG, Shi P-Y. 2015. The dengue virus NS5 protein as a target

for drug discovery. Antiviral Res 119:57–67. https://doi.org/10.1016/j.antiviral.2015.04.010.

19. Ray D, Shah A, Tilgner M, Guo Y, Zhao Y, Dong H, Deas TS, Zhou Y, Li H, Shi P-Y. 2006. West Nile virus 5′-cap structure is formed by sequential guanine N-7 and ribose 2′-O methylations by nonstructural protein 5. J Virol 80:8362–8370. https://doi.org/10.1128/JVI.00814-06.

20. Barral K, Sallamand C, Petzold C, Coutard B, Collet A, Thillier Y, Zimmermann J, Vasseur JJ, Canard B, Rohayem J, Debart F, Decroly E. 2013. Development of specific dengue virus 2′-O- and N7-methyltransferase assays for antiviral drug screening. Antiviral Res 99:292–300. https://doi.org/10.1016/j.antiviral.2013.06.001.

21. Dong H, Chang DC, Hua MHC, Lim SP, Chionh YH, Hia F, Lee YH, Kukkaro P, Lok S-M, Dedon PC, Shi P-Y. 2012. 2′-O methylation of internal adenosine by flavivirus NS5 methyltransferase. PLoS Pathog 8:e1002642. https://doi.org/10.1371/journal.ppat.1002642.

22. Coloma J, Jain R, Rajashankar KR, García-Sastre A, Aggarwal AK. 2016. Structures of NS5 methyltransferase from Zika virus. Cell Rep 16:3097–3102. https://doi.org/10.1016/j.celrep.2016.08.091.

23. Bollati M, Alvarez K, Assenberg R, Baronti C, Canard B, Cook S, Coutard B, Decroly E, de Lamballerie X, Gould EA, Grard G, Grimes JM, Hilgenfeld R, Jansson AM, Malet H, Mancini EJ, Mastrangelo E, Mattevi A, Milani M, Moureau G, Neyts J, Owens RJ, Ren J, Selisko B, Speroni S, Steuber H, Stuart DI, Unge T, Bolognesi M. 2010. Structure and functionality in flavivirus NS-proteins: perspectives for drug design. Antiviral Res 87:125–148. https://doi.org/10.1016/j.antiviral.2009.11.009.

24. Yap LJ, Luo D, Chung KY, Lim SP, Bodenreider C, Noble C, Shi P-Y, Lescar J. 2010. Crystal structure of the dengue virus methyltransferase bound to a 5′-capped octameric RNA. PLoS One 5:e12836. https://doi.org/10.1371/journal.pone.0012836.

25. Zhao Y, Soh TS, Lim SP, Chung KY, Swaminathan K, Vasudevan SG, Shi P-Y, Lescar J, Luo D. 2015. Molecular basis for specific viral RNA recognition and 2′-O-ribose methylation by the dengue virus nonstructural protein 5 (NS5). Proc Natl Acad Sci U S A 112:14834–14839. https://doi.org/10.1073/pnas.1514978112.

26. Milani M, Mastrangelo E, Bollati M, Selisko B, Decroly E, Bouvet M, Canard B, Bolognesi M. 2009. Flaviviral methyltransferase/RNA interaction: structural basis for enzyme inhibition. Antiviral Res 83:28–34. https://doi.org/10.1016/j.antiviral.2009.03.001.

27. Lim SP, Sonntag LS, Noble C, Nilar SH, Ng RH, Zou G, Monaghan P, Chung KY, Dong H, Liu B, Bodenreider C, Lee G, Ding M, Chan WL, Wang G, Jian YL, Chao AT, Lescar J, Yin Z, Vedananda TR, Keller TH, Shi PY. 2011. Small molecule inhibitors that selectively block dengue virus methyltransferase. J Biol Chem 286:6233–6240. https://doi.org/10.1074/jbc.M110.179184.

28. Brecher M, Chen H, Liu B, Banavali NK, Jones SA, Zhang J, Li Z, Kramer LD, Li H. 2015. Novel broad spectrum inhibitors targeting the flavivirus methyltransferase. PLoS One 10:e0130062. https://doi.org/10.1371/journal.pone.0130062.

29. Idrus S, Tambunan U, Zubaidi AA. 2012. Designing cyclopentapeptide inhibitor as potential antiviral drug for dengue virus ns5 methyltransferase. Bioinformation 8:348–352. https://doi.org/10.6026/97320630008348.

30. Coutard B, Decroly E, Li C, Sharff A, Lescar J, Bricogne G, Barral K. 2014. Assessment of dengue virus helicase and methyltransferase as targets for fragment-based drug discovery. Antiviral Res 106:61–70. https://doi.org/10.1016/j.antiviral.2014.03.013.

31. Benmansour F, Trist I, Coutard B, Decroly E, Querat G, Brancale A, Barral K. 2017. Discovery of novel dengue virus NS5 methyltransferase nonnucleoside inhibitors by fragment-based drug design. Eur J Med Chem 125:865–880. https://doi.org/10.1016/j.ejmech.2016.10.007.

32. Jansson AM, Jakobsson E, Johansson P, Lantez V, Coutard B, De Lamballerie X, Unge T, Jones TA. 2009. Structure of the methyltransferase domain from the Modoc virus, a flavivirus with no known vector. Acta Crystallogr Sect D Biol Crystallogr 65:796–803. https://doi.org/10.1107/S0907444909017260.

33. Selisko B, Peyrane FF, Canard B, Alvarez K, Decroly E. 2010. Biochemical characterization of the (nucleoside-2′O)-methyltransferase activity of dengue virus protein NS5 using purified capped RNA oligonucleotides 7MeGpppACn and GpppACn. J Gen Virol 91:112–121. https://doi.org/10.1099/vir.0.015511-0.

34. Egloff MP, Decroly E, Malet H, Selisko B, Benarroch D, Ferron F, Canard B. 2007. Structural and functional analysis of methylation and 5′-RNA sequence requirements of short capped RNAs by the methyltransferase

35. domain of dengue virus NS5. J Mol Biol 372:723–736. https://doi.org/10.1016/j.jmb.2007.07.005.

35. Erlanson DA, Fesik SW, Hubbard RE, Jahnke W, Jhoti H. 2016. Twenty years on: the impact of fragments on drug discovery. Nat Rev Drug Discov 15:605–619. https://doi.org/10.1038/nrd.2016.109.

36. Klema VJ, Ye M, Hindupur A, Teramoto T, Gottipati K, Padmanabhan R, Choi KH. 2016. Dengue virus nonstructural protein 5 (NS5) assembles into a dimer with a unique methyltransferase and polymerase interface. PLoS Pathog 12:e1005451. https://doi.org/10.1371/journal.ppat.1005451.

37. Zhao Y, Soh TS, Zheng J, Chan KWK, Phoo WW, Lee CC, Tay MYF, Swaminathan K, Cornvik TC, Lim SP, Shi PY, Lescar J, Vasudevan SG, Luo D. 2015. A crystal structure of the dengue virus NS5 protein reveals a novel inter-domain interface essential for protein flexibility and virus replication. PLoS Pathog 11:e1004682. https://doi.org/10.1371/journal.ppat.1004682.

38. Zhao Y, Soh TS, Ki Chan KW, Yin Fung SS, Swaminathan K, Lim SP, Shi P-Y, Huber T, Lescar J, Luo D, Vasudevan SG. 2015. Flexibility of NS5 methyltransferase-polymerase linker region is essential for dengue virus replication. J Virol 89:10717–10721. https://doi.org/10.1128/JVI.01239-15.

39. Lu G, Gong P. 2013. Crystal structure of the full-length Japanese encephalitis virus NS5 reveals a conserved methyltransferase-polymerase interface. PLoS Pathog 9:e1003549. https://doi.org/10.1371/journal.ppat.1003549.

40. Potisopon S, Priet S, Collet A, Decroly E, Canard B, Selisko B. 2014. The methyltransferase domain of dengue virus protein NS5 ensures efficient RNA synthesis initiation and elongation by the polymerase domain. Nucleic Acids Res 42:11642–11656. https://doi.org/10.1093/nar/gku666.

41. Brecher M, Chen H, Li Z, Banavali NK, Jones SA, Zhang J, Kramer LD, Li H. 2015. Identification and characterization of novel broad-spectrum inhibitors of the flavivirus methyltransferase. ACS Infect Dis 1:340–349. https://doi.org/10.1021/acsinfecdis.5b00070.

42. Lavergne T, Bertrand JR, Vasseur JJ, Debart F. 2008. A base-labile group for 2′-OH protection of ribonucleosides: a major challenge for RNA synthesis. Chemistry 14:9135–9138. https://doi.org/10.1002/chem.200801392.

43. Zlatev I, Lavergne T, Debart F, Vasseur JJ, Manoharan M, Morvan F. 2010. Efficient solid-phase chemical synthesis of 5′-triphosphates of DNA, RNA, and their analogues. Org Lett 12:2190–2193. https://doi.org/10.1021/ol1004214.

44. Thillier Y, Decroly E, Morvan F, Canard B, Vasseur J-J, Debart F. 2012. Synthesis of 5′ cap-0 and cap-1 RNAs using solid-phase chemistry coupled with enzymatic methylation by human (guanine-N7)-methyl transferase. RNA 18:856–868. https://doi.org/10.1261/rna.030932.111.

45. Vonrhein C, Flensburg C, Keller P, Sharff A, Smart O, Paciorek W, Womack T, Bricogne G. 2011. Data processing and analysis with the autoPROC toolbox. Acta Crystallogr Sect D Biol Crystallogr 67:293–302. https://doi.org/10.1107/S0907444911007773.

46. Kabsch W. 2010. Xds. Acta Crystallogr Sect D Biol Crystallogr 66:125–132. https://doi.org/10.1107/S0907444909047337.

47. Evans PR, Murshudov GN. 2013. How good are my data and what is the resolution? Acta Crystallogr Sect D Biol Crystallogr 69:1204–1214. https://doi.org/10.1107/S0907444913000061.

48. McCoy AJ, Grosse-Kunstleve RW, Adams PD, Winn MD, Storoni LC, Read RJ. 2007. Phaser crystallographic software. J Appl Crystallogr 40:658–674. https://doi.org/10.1107/S0021889807021206.

49. Langer G, Cohen SX, Lamzin VS, Perrakis A. 2008. Automated macromolecular model building for X-ray crystallography using ARP/wARP version 7. Nat Protoc 3:1171–1179. https://doi.org/10.1038/nprot.2008.91.

50. Bricogne G, Blanc E, Brandl M, Flensburg C, Keller P, Paciorek W, Roversi P, Sharff A, Smart OS, Vonrhein C, Womack TO. 2011. BUSTER version 2.11.2. Global Phasing Ltd, Cambridge, United Kingdom.

51. Emsley P, Lohkamp B, Scott WG, Cowtan K. 2010. Features and development of Coot. Acta Crystallogr Sect D Biol Crystallogr 66:486–501. https://doi.org/10.1107/S0907444910007493.

52. Davis IW, Leaver-Fay A, Chen VB, Block JN, Kapral GJ, Wang X, Murray LW, Arendall WB, Snoeyink J, Richardson JS, Richardson DC. 2007. MolProbity: all-atom contacts and structure validation for proteins and nucleic acids. Nucleic Acids Res 35(Web Server issue):W375–W383.

53. Krissinel E. 2012. Enhanced fold recognition using efficient short fragment clustering. J Mol Biochem 1:76–85.